Integration of Preventive and Emergency Responses for Power Grid Resilience Enhancement

Gang Huang, *Student Member, IEEE*, Jianhui Wang, *Senior Member, IEEE*, Chen Chen, *Member, IEEE*, Junjian Qi, *Member, IEEE*, and Chuangxin Guo, *Senior Member, IEEE*

***Abstract*—Boosting the resilience of power systems is one of the core requirements of smart grid. In this paper, an integrated resilience response framework is proposed, which not only links the situational awareness with resilience enhancement, but also provides effective and efficient responses in both preventive and emergency states. The core of the proposed framework is a two-stage robust mixed-integer optimization model, whose mathematical formulation is presented in this paper as well. To solve the above model, an algorithm based on the nested column-and-constraint generation decomposition is provided, and computational efficiency improvement techniques are proposed. Preventive response in this paper considers generator re-dispatch and topology switching, while emergency response includes generator re-dispatch, topology switching and load shedding. Several numerical simulations validate the effectiveness of the proposed framework and the efficiency of the solution methodology. Key findings include the following: 1) in terms of enhancing power grid resilience, the integrated resilience response is preferable to both independent preventive response and independent emergency response; 2) the power grid resilience could be further enhanced by utilizing topology switching in the integrated resilience response.**

***Index Terms*—Blackouts, emergency response, generator re-dispatch, integrated resilience response, load shedding, natural disasters, optimization, preventive response, resilience, resilience definition, resilience enhancement, resiliency, robust optimization, situational awareness, topology switching.**

I. Introduction

As a direct impact of climate change, the frequency and intensity of natural disasters have largely increased over the past decades and are expected to continuously increase in the future [1]. Natural disasters can cause power outages; in fact, they are the leading cause of blackouts (e.g., 80% of all major power outages between 2003-2012 were caused by natural disasters [2]), which affect millions of people and cost the U.S. economy alone billions of dollars each year [3]. With other infrastructures and our society as a whole increasingly depending on electricity [4], it is vitally important to provide continuous electric power, especially against natural disasters.

To make the power grid stronger and smarter against natural disasters, the concept of resilience was recently introduced [3]–[7]. It is different from the concept of reliability; the focus of reliability is on high-probability events, while the focus of resilience is on high-impact events. However, although there is wide agreement in both academia and industry that power grid resilience enhancement is of key importance [3], [5]–[7], there is no agreement yet on the resilience definition. In the literature, over 70 definitions for resilience can be found in different disciplines [8], and some of them are completely different from others. But, as [8] pointed out, these definitions vary between two features: adaptation and recovery. Here, by "adaptation" we mean the process of changing in oder to make the system suitable for a new situation, and "recovery" means the process of returning to a normal condition after a period of disturbance. In the context of power systems, these two features could also be found among all the different definitions [4]–[7]. Thus, in this paper, we propose defining the power grid resilience as the ability of power grids to adapt to disaster scenarios and recover to pre-disaster states.

Based on the above definition of resilience, resilience enhancement strategies could be categorized into two groups: enhancing the adaptation ability and enhancing the recovery ability. On the other hand, following the traditional classification of power system practices, these strategies can also be categorized from the perspective of planning and from the perspective of operation, while the operation strategies can be further divided by the three operating states—preventive state, emergency state, and restorative state [9]—that power grids will go through. As a result, we have in total four types of power grid resilience enhancement strategies (i.e., resilience planning, preventive response, emergency response, and resilience restoration), as depicted in Fig. 1.

Generally, resilience planning includes hardening [3], vegetation management [10], distributed generation resource allocation [11], and so forth. These are important to enhance power grid resilience, but this paper will focus on the operation

Manuscript received May 29, 2016; revised November 5, 2016 and February 4, 2017; accepted March 18, 2017. Date of publication March 22, 2017; date of current version October 18, 2017. This work is supported in part by the Key Program of National Natural Science Foundation of China under Grant 51537010, in part by the National Basic Research Program (973 Program) under Grant 2013CB228206, in part by the China Scholarship Council, and in part by the U.S. Department of Energy's Office of Electrical Delivery and Energy Reliability. Paper no. TPWRS-00810-2016.

G. Huang and C. Guo are with the College of Electrical Engineering, Zhejiang University, Hangzhou, Zhejiang 310027, China (e-mail: huanggang@zju.edu.cn; guochuangxin@zju.edu.cn).

J. Wang is with the Department of Electrical Engineering, Southern Methodist University, Dallas, TX 75205 USA, and also with the Energy Systems Division, Argonne National Laboratory, Argonne, IL 60439 USA (e-mail: jianhui.wang@ieee.org).

C. Chen and J. Qi are with the Energy Systems Division, Argonne National Laboratory, Argonne, IL 60439 USA (e-mail: morningchen@anl.gov; jqi@anl.gov).

Color versions of one or more of the figures in this paper are available online at http://ieeexplore.ieee.org.

Digital Object Identifier 10.1109/TPWRS.2017.2685640

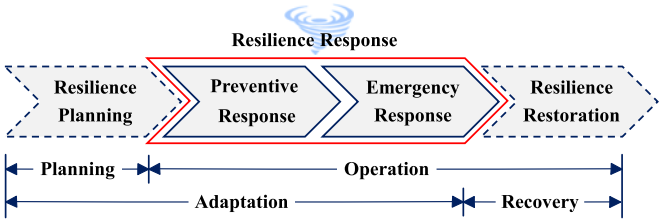

Fig. 1. The milestones of resilience enhancement strategies. Here, the scope of this paper is outlined in the red arrow shape, and the blue storm image indicates natural disasters.

strategies, because they as the "smarter" measures could provide more specific and therefore more cost-effective strategies than resilience planning [6]. Resilience restoration will also not be discussed here, as the focus of this paper is on the adaptation ability of power grids. There are many interesting works on the resilience restoration, and readers interested in it are referred to [7], [12], [13]. To conclude, this paper aims to enhance the resilience adaptation ability of power grids from the perspective of operation. Therefore only preventive response and emergency response, which can be collectively called resilience response, will be included. The red arrow shape in Fig. 1 shows the scope of this paper.

In general, preventive response is comprised of the actions available before disaster scenarios unfold, and emergency response comprises the actions taken in the aftermath of a disaster. For simplicity, only the indispensable components of power grids (i.e., generators, transmission lines, and loads) will be taken into account in this paper, and other facilities, for example, the emerging energy storage [14], are not considered. Accordingly, the specific strategies we will consider include generator re-dispatch, topology switching, and load shedding. As power grids in the preventive state are being operated to satisfy all the demands without violating any operating constraints [9], load shedding is considered only in the emergency state. Generator re-dispatch and topology switching can be utilized in both preventive and emergency states, but evidently the emergency state will have fewer resources than the preventive state. Nevertheless, although preventive response and emergency response both have resources to enhance power grid resilience, they are traditionally deployed independently.

To further enhance the power grid resilience, this paper proposes integrating the preventive response and emergency response. Other models that boost the power grid resilience from the perspective of operation can also be found in the literature [15]–[20], but they mainly utilize only independent emergency response. Independent preventive response is often not adequate to keep the generation-demand balance after natural disasters unfold, and this will be verified in Section V. On the other hand, the topology switching we will investigate is also distinguished from that in the literature. The widely discussed topology switching in the literature is in fact the in-service lines (ISLs) switch off [21]–[26], but with the development of new facilities against natural disasters, the out-of-service lines (OSLs) switch on (e.g., the backup transmission lines [27]) has emerged, and this will be considered along with the ISLs switch off in this paper. Other possible implementations of OSLs switch on in the preventive state include: 1) restoring the outage-scheduled transmission lines [28], 2) rescheduling or canceling the outage schedules [29].

The main contributions of this paper are as follows:

1) An integrated resilience response (IRR) framework is proposed to integrate the preventive response and emergency response. With the proposed IRR framework, situational awareness and resilience enhancement are directly linked.
2) The mathematical formulation of the core of the proposed IRR framework, which is a two-stage robust mixed-integer optimization (RoMIO) model, is proposed to support the decision-making process. With the RoMIO model, both the preventive response strategy and the emergency response strategy can be derived.
3) To solve the RoMIO model, a solution methodology based on the nested column-and-constraint generation decomposition is presented, and computational efficiency improvement techniques are also provided.

Through the research conducted in this paper, two key findings can be made:

1) In terms of enhancing power grid resilience, the integrated resilience response is preferable to both independent preventive response and independent emergency response.
2) The power grid resilience could be further enhanced by utilizing topology switching in the integrated resilience response.

The remainder of this paper is organized as follows. Section II describes the IRR framework. Section III presents the mathematical formulation of the RoMIO model. Section IV gives the solution methodology for the RoMIO model. Section V provides case studies along with analysis. Section VI contains a brief discussion of practical implications. The conclusion is drawn in Section VII.

II. Conceptual Framework

The IRR framework is based on the situational awareness, which will be discussed in Section II-A. Then, conceptual framework of the IRR will be given in Section II-B.

A. Situational Awareness

Situational awareness provides critical information about power grids and natural disasters, which is the foundation for resilience response decision making. In the situational awareness, power outage prediction is of vital importance because it connects power grids to natural disasters.

Power outage prediction is a multidisciplinary research field. It is often accomplished through the development of power outage prediction models based on parameters of natural disasters. For example, to predict storm-related power outages, storm data including wind, rainfall, and storm surge are used as inputs to a regression model in [30]. Since this paper aims to investigate the resilience response strategies based on the results of power outage prediction, we here do not specify the particular prediction model or disaster data that are used to predict power outages;

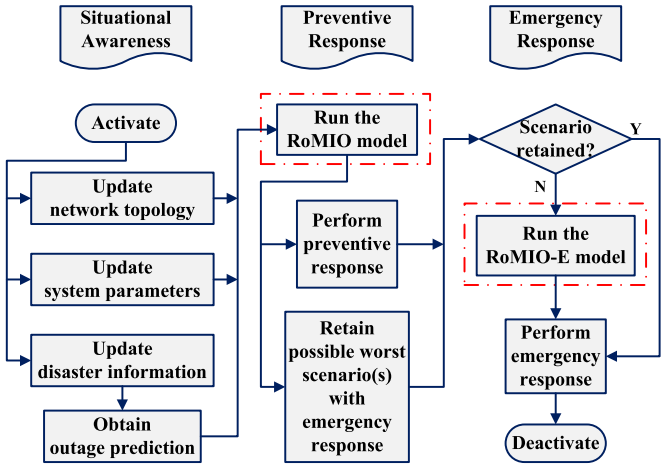

Fig. 2. The integrated resilience response framework.

instead, we focus on the damage from natural disasters in this paper. The storm will be used as an example, as it is one of the most severe natural disasters [7].

While there is an underlying assumption in this paper that the situational awareness is sufficient, insufficient situational awareness could also impact the power grid resilience. Generally, delayed, incorrect or deficient resilience response may be derived with insufficient situational awareness. This is another interesting topic for research, and readers that are interested in it are referred to [31]–[33].

B. The Integrated Resilience Response Framework

Based on the situational awareness, here we propose the IRR framework to enhance power grid resilience. The flow chart of the framework is depicted in Fig. 2, and the response process is summarized as follows:

1) *Situational awareness:* Activate the IRR framework when the disaster is brewing. Update the disaster forecast information from national meteorological services or local weather forecast offices, and obtain the power outage prediction based on it. Gather the obtained power outage prediction results and the latest information of power grids (including the network topology and system parameters), and they will serve as inputs to the next stage.
2) *Preventive response:* Run the RoMIO model, whose mathematical formulation will be presented in Section III, to derive effective preventive and emergency response strategies. Speedily perform the derived preventive response when it is available, and retain the emergency response strategies in accord with possible worst disaster scenario(s) for the next stage.
3) *Emergency response:* Check whether the realized disaster scenario is retained during the preventive response stage. If retained, the corresponding emergency response strategy previously derived from the RoMIO model will be immediately performed; otherwise, run the RoMIO-E model, which is the emergency response module of the RoMIO model and will be presented in Section III as well, then perform the derived emergency response. When the emergency response has been performed, deactivate the framework for future use.

Considering the provided data from SCADA and WAMS, in this paper we will take into account the following system parameters: loads at each bus, initial generator outputs, generator capacities, generator ramp-up limits, transmission line capacities, and transmission line parameters. The network topology data that we will take into account include the bus locations and the transmission line status.

Some natural disasters can sweep across a large area for a relatively long period of time. To capture this spatial and temporal dynamics of natural disasters, time horizon should be considered in the IRR framework, and the above response process could then work in a rolling manner. But here we will focus on the integration of preventive and emergency responses without introducing the rolling mode, thus no time horizon will be considered in this paper.

III. Mathematical Formulation

The mathematical formulation of the RoMIO model is presented in this section. Sections III-A–III-C pertain to the modeling of preventive response, damage from natural disasters, and emergency response, respectively. The entire RoMIO model and its abstract mathematical formulation are given in Section III-D.

A. Preventive Response

As previously mentioned, power grids in the preventive state are being operated to satisfy all the demands without violating any operating constraints. From an economic point of view, the minimum-cost operating point of the system is optimal. But to enhance the power grid resilience, the load shedding cost in the emergency state should also be considered during the preventive state. Hence the objective of the preventive response in the RoMIO model is:

$$\min \sum_{g\in\mathcal{G}} c_g p_g^a + \sum_{d\in\mathcal{D}} c_d p_{d,s}^c, \tag{1}$$

where c_g is the offer price of generator g, c_d is the shedding price of load d, p_g^a is the power output of generator g in the preventive state, and $p_{d,s}^c$ is the power shed of load d in the emergency state.

Based on the traditional DC power flow model, the power balance within power grids is described as follows:

$$\sum_{g\in\mathcal{G}_i} p_g^a - \sum_{(i,j)\in\mathcal{L}_i} p_{ij}^a = \sum_{d\in\mathcal{D}_i} P_d, i \in \mathcal{B} \tag{2}$$

$$(s_{ij}^a - 1)M_{ij} \le p_{ij}^a + B_{ij}\theta_{ij}^a \le (1 - s_{ij}^a)M_{ij}, (i,j) \in \mathcal{L}, \tag{3}$$

where (2) represents power balance constraints for each bus, and (3) represents power balance constraints for each transmission line. Note that the modeling of topology switching has already been included in (3). Here, generator output p_g^a and transmission line status s_{ij}^a are independent variables, line flow p_{ij}^a and voltage angle θ_i^a are dependent variables. P_d is the power demand of load d, $B_{ij} = -1/X_{ij}$, where X_{ij} is the reactance of

transmission line (i, j), and M_{ij} is a big M constant for transmission line (i, j), which can be easily chosen, for example, by $M_{ij} = P_{ij}^{\max} - B_{ij}(\Theta_i^{\max} - \Theta_j^{\min})$.

Following the convention in [23], [24], [34], each generator capacity is limited as follows:

$$p_g^a \leq P_g^{\max}, g \in \mathcal{G}. \tag{4}$$

In addition, the generators are subject to ramp-up constraints:

$$p_g^a - p_g^0 \leq P_g^{a,\max}, g \in \mathcal{G}. \tag{5}$$

Here, $P_g^{\max}$ is the generator capacity, p_g^0 is the initial generator output, and $P_g^{a,\max}$ is the generator ramp-up capacity in the preventive state. The ramp-down constraints are ignored, as the focus of this paper is on power grid damage induced by natural disasters, which cause capacity deficiencies, not surpluses [34].

Each transmission line is limited as follows:

$$-P_{ij}^{\max} s_{ij}^a \leq p_{ij}^a \leq P_{ij}^{\max} s_{ij}^a, (i, j) \in \mathcal{L}, \tag{6}$$

and each bus should meet the voltage angle limits:

$$\Theta_i^{\min} \leq \theta_i^a \leq \Theta_i^{\max}, i \in \mathcal{B}. \tag{7}$$

Furthermore, although the resources are usually less limited in the preventive state than that in the emergency state, the number of ISLs that we can switch off and the number of OSLs that we can switch on are still limited against natural disasters. As a result, we have:

$$\sum_{(i,j)\in\mathcal{L}} s_{ij}^0 (1 - s_{ij}^a) \leq K_I^a \tag{8}$$

$$\sum_{(i,j)\in\mathcal{L}} (1 - s_{ij}^0) s_{ij}^a \leq K_O^a, \tag{9}$$

where s_{ij}^0 represents the initial state of transmission line (i, j), K_I^a and K_O^a are the quantity limits for the ISLs switch off and OSLs switch on respectively. After the employment of preventive response, transmission line (i, j) is in service if $s_{ij}^a = 1$ and out of service if $s_{ij}^a = 0$.

B. Damage From Natural Disasters

Damage from natural disasters can cause load shedding, and the worst disaster scenario satisfies the following function:

$$\max \sum_{d\in\mathcal{D}} p_{d,s}^c. \tag{10}$$

Based on the natural disaster information, statistical models and simulation models can be utilized to predict power outages. This process corresponds to the situational awareness, which we previously discussed in Section II. As the focus of this paper is on investigating the resilience response strategies based on the results of power outage prediction, we do not specify the particular prediction model or disaster data that are used to predict power outages. Instead, we focus on the damage from natural disasters in this paper. For brevity, the damage from storms will be modeled here.

As the strength of storms could be reflected by the number of damaged transmission lines [11], and many existing works (e.g., [30]) that aim to assess the impact of storms on power grids using statistical methods also estimate the aggregated number of damage within a given area, we here assume the strength of storms is predictable and the estimated maximum number of damaged transmission lines is known. Accordingly, the damage from storms can be modeled by an uncertainty set based on the estimated maximum number of damaged transmission lines as follows:

$$\sum_{(i,j)\in\mathcal{L}} (1 - s_{ij}^b) \leq K^b, \tag{11}$$

where K^b is the estimated maximum number of damaged transmission lines, $s_{ij}^b = 0$ indicates that line (i, j) will be damaged and $s_{ij}^b = 1$ indicates it will not be damaged.

The uncertainty set based on K^b is used because it is a tractable method given that the statistical information of damaged transmission lines is difficult to obtain. We here model the transmission lines because they are the most commonly damaged electricity infrastructures against storms [35]. The damage from other natural disasters could be similarly modeled. Specifically, for those natural disasters that have similar effects of storms and will damage transmission lines (e.g., icing), a similar uncertainty set based on the estimated maximum number of damaged transmission lines could be formulated to model the damage; for other natural disasters that will affect other components (e.g., flooding mainly affects the generators rather than the transmission lines), an uncertainty set based on the estimated maximum number of other damaged components could then be utilized to model the damage. In the latter case, we mention that the status of other components may be introduced, and the RoMIO model should be relevantly modified to adapt to this change.

This paper assumes the situational awareness is sufficient and the estimated maximum number of damaged transmission lines is known. Considering K^b with uncertainty and modeling the damage from natural disasters in a different way are other issues that will be interesting to research.

C. Emergency Response

After natural disasters unfold, power grids enter the emergency state and should be operated to satisfy as many demands as possible. Thus, the objective becomes:

$$\min \sum_{d\in\mathcal{D}} p_{d,s}^c. \tag{12}$$

The power balance constraints of the system are similar to that in the preventive state:

$$\sum_{g\in\mathcal{G}_i} p_g^c - \sum_{(i,j)\in\mathcal{L}_i} p_{ij}^c + \sum_{d\in\mathcal{D}_i} p_{d,s}^c = \sum_{d\in\mathcal{D}_i} P_d, i \in \mathcal{B} \tag{13}$$

$$(s_{ij}^c - 1) M_{ij} \leq p_{ij}^c + B_{ij}\theta_{ij}^c \leq (1 - s_{ij}^c) M_{ij}, (i, j) \in \mathcal{L} \tag{14}$$

where generator output p_g^c, transmission line status s_{ij}^c, and power shed $p_{d,s}^c$ are independent variables, line flow p_{ij}^c and voltage angle θ_i^c are dependent variables; the rest of the symbols are consistent with that in the preventive state.

Similar to the preventive state, each generator capacity is limited as follows:

$$p_g^c \le P_g^{\max}, g \in \mathcal{G}, \tag{15}$$

and the generators are subject to emergency state ramp-up constraints:

$$p_g^c - p_g^a \le P_g^{c,\max}, g \in \mathcal{G}. \tag{16}$$

Note that the ramp-up constraints for emergency state are not the same as that for preventive state, because generators in the emergency state will usually have shorter time to ramp up. Generally, we have $P_g^{c,\max} \le P_g^{a,\max}$.

Each transmission line and each bus are limited similarly to that in the preventive state:

$$-P_{ij}^{\max} s_{ij}^c \le p_{ij}^c \le P_{ij}^{\max} s_{ij}^c, (i,j) \in \mathcal{L} \tag{17}$$

$$\Theta_i^{\min} \le \theta_i^c \le \Theta_i^{\max}, i \in \mathcal{B}. \tag{18}$$

In addition, the following constraints are involved when the load shedding is performed:

$$0 \le p_{d,s}^c \le P_d, d \in \mathcal{D}. \tag{19}$$

The constraints for ISLs switch off and OSLs switch on in the emergency state are given as follows:

$$\sum_{(i,j)\in\mathcal{L}} s_{ij}^a s_{ij}^b (1 - s_{ij}^c) \le K_I^c \tag{20}$$

$$\sum_{(i,j)\in\mathcal{L}} (1 - s_{ij}^a) s_{ij}^b s_{ij}^c \le K_O^c \tag{21}$$

$$s_{ij}^c \le s_{ij}^b, (i,j) \in \mathcal{L}, \tag{22}$$

where K_I^c and K_O^c are the quantity limits for ISLs switch off and OSLs switch on in the emergency state. After the employment of emergency response, transmission line (i,j) is in service if $s_{ij}^c = 1$ and out of service if $s_{ij}^c = 0$.

Furthermore, as the emergency state has fewer resilience resources than the preventive state, the emergency state may have not only tighter ramp-up capacities for generators (i.e., $P_g^{c,\max} \le P_g^{a,\max}$), but also tighter switching limits for transmission lines. To reflect this difference in topology switching limits, we assume that the OSLs in the preventive state are unavailable to the emergency state, and emergency response could only switch on the lines that are previously switched off by the preventive response. Another reason behind this assumption is that some sources of OSLs in the preventive state, for example, restoring the outage-scheduled transmission lines [28], need a relatively long time that the emergency state cannot afford. Thus, we have:

$$s_{ij}^c \le s_{ij}^0 + s_{ij}^a, (i,j) \in \mathcal{L}. \tag{23}$$

D. Integration of Preventive and Emergency Responses

Based on Sections III-A–III-C, the entire RoMIO model can be given as follows:

$$\begin{aligned} \min \quad & (1) \\ \text{s.t.} \quad & (2)-(9) \\ & \max \quad (10) \\ & \text{s.t.} \quad (11) \\ & \qquad \min \quad (12) \\ & \qquad \text{s.t.} \quad (13)-(23). \end{aligned} \tag{24}$$

However, it is difficult to directly solve the above model, because there are quadratic terms and cubic terms in (20)–(21). To deal with this issue, we introduce binary variables $s_{ij,1} = s_{ij}^a s_{ij}^b$, $s_{ij,2} = s_{ij}^b s_{ij}^c$, and $s_{ij,3} = s_{ij}^a s_{ij}^b s_{ij}^c$, then (20)–(21) become:

$$\sum_{(i,j)\in\mathcal{L}} (s_{ij,1} - s_{ij,3}) \le K_I^c \tag{25}$$

$$\sum_{(i,j)\in\mathcal{L}} (s_{ij,2} - s_{ij,3}) \le K_O^c, \tag{26}$$

where $s_{ij,1}$, $s_{ij,2}$, and $s_{ij,3}$ are all products of multiple binary variables, and they can be linearized by:

$$s = \prod_{k\in\mathcal{N}} s_k \iff \begin{cases} s \le s_k, k \in \mathcal{N} \\ s \ge \sum_{k\in\mathcal{N}} s_k - \text{card}(\mathcal{N}) + 1, \end{cases} \tag{27}$$

where $\text{card}(\cdot)$ is the number of elements in a set, and s_k ($k \in \mathcal{N}$) and s are binary variables.

Due to the above relaxation, the objective functions and constraint functions of the RoMIO model become either linear or mixed-integer linear now. Its abstract mathematical formulation can be given as follows:

$$\begin{aligned} \min_{\boldsymbol{s}_1, \boldsymbol{x}_1} \quad & \boldsymbol{c}_1^{\mathrm{T}} \boldsymbol{x}_1 + \boldsymbol{c}_3^{\mathrm{T}} \boldsymbol{x}_3 \\ \text{s.t.} \quad & \boldsymbol{A}_1 \left[\begin{array}{cc} \boldsymbol{s}_1^{\mathrm{T}} & \boldsymbol{x}_1^{\mathrm{T}} \end{array} \right]^{\mathrm{T}} \le \boldsymbol{b}_1 \\ & \max_{\boldsymbol{s}_2} \quad \boldsymbol{c}_3^{\mathrm{T}} \boldsymbol{x}_3 \\ & \text{s.t.} \quad \boldsymbol{A}_2 \boldsymbol{s}_2 \le \boldsymbol{b}_2 \\ & \qquad \min_{\boldsymbol{s}_3, \boldsymbol{x}_3} \quad \boldsymbol{c}_3^{\mathrm{T}} \boldsymbol{x}_3 \\ & \qquad \text{s.t.} \quad \boldsymbol{A}_3 \left[\begin{array}{ccccc} \boldsymbol{s}_1^{\mathrm{T}} & \boldsymbol{x}_1^{\mathrm{T}} & \boldsymbol{s}_2^{\mathrm{T}} & \boldsymbol{s}_3^{\mathrm{T}} & \boldsymbol{x}_3^{\mathrm{T}} \end{array} \right]^{\mathrm{T}} \le \boldsymbol{b}_3, \end{aligned} \tag{28}$$

where $\boldsymbol{s}_1$, $\boldsymbol{x}_1$, $\boldsymbol{s}_2$, $\boldsymbol{s}_3$, and $\boldsymbol{x}_3$ are made up of s_{ij}^a, $\{p_g^a, p_{ij}^a, \theta_i^a\}$, s_{ij}^b, $\{s_{ij}^c, s_{ij,1}, s_{ij,2}, s_{ij,3}\}$, and $\{p_g^c, p_{d,s}^c, p_{ij}^c, \theta_i^c\}$, respectively.

When natural disasters unfold, the first two levels of the tri-level problem (28) are determined, and only $\boldsymbol{s}_3$ and $\boldsymbol{x}_3$ remain undecided. This corresponds to the emergency response module of the RoMIO model, and we refer to it as the RoMIO-E model. Note that the RoMIO-E model is a single-level mixed-integer linear optimization model, which can be efficiently solved using the state-of-the-art MIP (i.e., mixed-integer linear programming) solvers. But the entire RoMIO model is much harder

to solve because it is a tri-level problem with binary decision variables in each level. In the next section, we will propose a solution methodology to solve it efficiently.

IV. Solution Methodology

The RoMIO model is a tri-level mixed-integer linear optimization problem, and the nested column-and-constraint generation (NC&CG) decomposition framework proposed in [36] is able to solve this kind of problem. However, a general algorithm based on the NC&CG decomposition can be very time-consuming, and this will impose practical limitations on the application of the IRR framework against natural disasters. In this section, we will present our solution methodology and the techniques we use to efficiently solve the RoMIO model.

A. NC&CG Decomposition-Based Algorithm

The tri-level problem (28) can be decomposed into a single-level min problem as the master problem and a bi-level max-min problem as the subproblem:

$$\begin{aligned}
\min_{\boldsymbol{s}_1,\boldsymbol{x}_1,\boldsymbol{s}_3^i,\boldsymbol{x}_3^i,\eta}\quad & \boldsymbol{c}_1^{\mathrm{T}}\boldsymbol{x}_1+\eta \\
\text{s.t.}\quad & \boldsymbol{c}_3^{\mathrm{T}}\boldsymbol{x}_3^i\le\eta \\
& \boldsymbol{A}_1\left[\begin{array}{cc}\boldsymbol{s}_1^{\mathrm{T}} & \boldsymbol{x}_1^{\mathrm{T}}\end{array}\right]^{\mathrm{T}}\le\boldsymbol{b}_1 \qquad \text{(MP-I)}\\
& \boldsymbol{A}_3\left[\begin{array}{ccccc}\boldsymbol{s}_1^{\mathrm{T}} & \boldsymbol{x}_1^{\mathrm{T}} & \boldsymbol{s}_2^{*i\mathrm{T}} & \boldsymbol{s}_3^{i\mathrm{T}} & \boldsymbol{x}_3^{i\mathrm{T}}\end{array}\right]^{\mathrm{T}}\le\boldsymbol{b}_3 \\
& \forall i\in\{1,\ldots,k\} \\
\max_{\boldsymbol{s}_2}\min_{\boldsymbol{s}_3,\boldsymbol{x}_3}\quad & \boldsymbol{c}_1^{\mathrm{T}}\boldsymbol{x}_1^*+\boldsymbol{c}_3^{\mathrm{T}}\boldsymbol{x}_3 \\
\text{s.t.}\quad & \boldsymbol{A}_2\boldsymbol{s}_2\le\boldsymbol{b}_2 \qquad \text{(SP-I)}\\
& \boldsymbol{A}_3\left[\begin{array}{ccccc}\boldsymbol{s}_1^{*\mathrm{T}} & \boldsymbol{x}_1^{*\mathrm{T}} & \boldsymbol{s}_2^{\mathrm{T}} & \boldsymbol{s}_3^{\mathrm{T}} & \boldsymbol{x}_3^{\mathrm{T}}\end{array}\right]^{\mathrm{T}}\le\boldsymbol{b}_3,
\end{aligned}$$

where (MP-I) and (SP-I) will be iteratively solved to provide the lower bound and upper bound for (28), respectively. Here, η is a newly introduced variable, k is the iteration number, and variables denoted by an asterisk $(*)$ in (MP-I) or (SP-I) represent the optimal values derived from each other. After each iteration, k is updated by adding 1, and new variables and constraints will be generated and added to (MP-I).

It has been proved that the above iteration will terminate in finite steps and the optimal value can be achieved [36]. Here, (MP-I) is a classical mixed-integer linear programming problem and can be directly solved with the state-of-the-art MIP solvers, but (SP-I) is a bi-level problem with integers in either level and cannot be straightforwardly solved. Thus, we rewrite (SP-I) in a tri-level form as follows:

$$\begin{aligned}
\max_{\boldsymbol{s}_2}\min_{\boldsymbol{s}_3}\min_{\boldsymbol{x}_3}\quad & \boldsymbol{c}_1^{\mathrm{T}}\boldsymbol{x}_1^*+\boldsymbol{c}_3^{\mathrm{T}}\boldsymbol{x}_3 \\
\text{s.t.}\quad & \boldsymbol{A}_2\boldsymbol{s}_2\le\boldsymbol{b}_2 \qquad (29)\\
& \boldsymbol{A}_3\left[\begin{array}{ccccc}\boldsymbol{s}_1^{*\mathrm{T}} & \boldsymbol{x}_1^{*\mathrm{T}} & \boldsymbol{s}_2^{\mathrm{T}} & \boldsymbol{s}_3^{\mathrm{T}} & \boldsymbol{x}_3^{\mathrm{T}}\end{array}\right]^{\mathrm{T}}\le\boldsymbol{b}_3.
\end{aligned}$$

Then it can be decomposed into the following master problem and subproblem, which will also be iteratively solved to provide upper bound and lower bound for (SP-I), respectively:

$$\begin{aligned}
\max_{\boldsymbol{s}_2,\boldsymbol{x}_3^j,\boldsymbol{\lambda}^j,\tau}\quad & \boldsymbol{c}_1^{\mathrm{T}}\boldsymbol{x}_1^*+\tau \\
\text{s.t.}\quad & \tau\le\boldsymbol{c}_3^{\mathrm{T}}\boldsymbol{x}_3^j \\
& \boldsymbol{A}_2\boldsymbol{s}_2\le\boldsymbol{b}_2 \\
& \boldsymbol{A}_3\left[\begin{array}{ccccc}\boldsymbol{s}_1^{*\mathrm{T}} & \boldsymbol{x}_1^{*\mathrm{T}} & \boldsymbol{s}_2^{\mathrm{T}} & \boldsymbol{s}_3^{*j\mathrm{T}} & \boldsymbol{x}_3^{j\mathrm{T}}\end{array}\right]^{\mathrm{T}}\le\boldsymbol{b}_3 \\
& \boldsymbol{A}_{3,5}^{\mathrm{T}}\boldsymbol{\lambda}^j=-\boldsymbol{c}_3 \qquad \text{(MP-II)}\\
& \boldsymbol{c}_3^{\mathrm{T}}\boldsymbol{x}_3^j=(\boldsymbol{A}_{3,1-4}\left[\begin{array}{ccccc}\boldsymbol{s}_1^{*\mathrm{T}} & \boldsymbol{x}_1^{*\mathrm{T}} & \boldsymbol{s}_2^{\mathrm{T}} & \boldsymbol{s}_3^{*j\mathrm{T}}\end{array}\right]^{\mathrm{T}}-\boldsymbol{b}_3)^{\mathrm{T}}\boldsymbol{\lambda}^j \\
& \boldsymbol{\lambda}^j\ge\boldsymbol{0} \\
& \forall j\in\{1,\cdots,k'\} \\
\min_{\boldsymbol{s}_3,\boldsymbol{x}_3}\quad & \boldsymbol{c}_1^{\mathrm{T}}\boldsymbol{x}_1^*+\boldsymbol{c}_3^{\mathrm{T}}\boldsymbol{x}_3 \qquad \text{(SP-II)}\\
\text{s.t.}\quad & \boldsymbol{A}_3\left[\begin{array}{ccccc}\boldsymbol{s}_1^{*\mathrm{T}} & \boldsymbol{x}_1^{*\mathrm{T}} & \boldsymbol{s}_2^{*\mathrm{T}} & \boldsymbol{s}_3^{\mathrm{T}} & \boldsymbol{x}_3^{\mathrm{T}}\end{array}\right]^{\mathrm{T}}\le\boldsymbol{b}_3,
\end{aligned}$$

where $\boldsymbol{\lambda}^j$ represents the dual variables of the constraint $\boldsymbol{A}_3\left[\begin{array}{ccccc}\boldsymbol{s}_1^{*\mathrm{T}} & \boldsymbol{x}_1^{*\mathrm{T}} & \boldsymbol{s}_2^{\mathrm{T}} & \boldsymbol{s}_3^{*j\mathrm{T}} & \boldsymbol{x}_3^{j\mathrm{T}}\end{array}\right]^{\mathrm{T}}\le\boldsymbol{b}_3$ in the (SP-II) problem, τ is a newly introduced variable, k' is the iteration number, and new variables and constraints will be generated and added to (MP-II) after each iteration. Note that $\left[\begin{array}{cc}\boldsymbol{A}_{3,1-4} & \boldsymbol{A}_{3,5}\end{array}\right]=\boldsymbol{A}_3$.

B. Computational Efficiency Improvement Techniques

Theoretically, both Karush-Kuhn-Tucker conditions (KKT) and strong duality theory (SDT) can be used in the NC&CG decomposition. But they will both introduce bilinear terms, and it is fundamentally more difficult to deal with bilinear terms than with linear ones. As a result, the algorithm can be effective, but not efficient, especially when a large number of bilinear terms are introduced.

When applying the KKT, bilinear terms are introduced due to the following constraint:

$$\left(\boldsymbol{b}_3-\boldsymbol{A}_3\left[\begin{array}{ccccc}\boldsymbol{s}_1^{*\mathrm{T}} & \boldsymbol{x}_1^{*\mathrm{T}} & \boldsymbol{s}_2^{\mathrm{T}} & \boldsymbol{s}_3^{*j\mathrm{T}} & \boldsymbol{x}_3^{j\mathrm{T}}\end{array}\right]^{\mathrm{T}}\right)\circ\boldsymbol{\lambda}^j=\boldsymbol{0}, \qquad (30)$$

where "$\circ$" denotes the component-wise multiplication.

When the SDT is applied, the constraint that introduces bilinear terms becomes:

$$\boldsymbol{c}_3^{\mathrm{T}}\boldsymbol{x}_3^j=\left(\boldsymbol{A}_{3,1-4}\left[\begin{array}{ccccc}\boldsymbol{s}_1^{*\mathrm{T}} & \boldsymbol{x}_1^{*\mathrm{T}} & \boldsymbol{s}_2^{\mathrm{T}} & \boldsymbol{s}_3^{*j\mathrm{T}} & \boldsymbol{x}_3^{j\mathrm{T}}\end{array}\right]^{\mathrm{T}}-\boldsymbol{b}_3\right)^{\mathrm{T}}\boldsymbol{\lambda}^j. \qquad (31)$$

We already have $\boldsymbol{A}_3=\left[\begin{array}{cc}\boldsymbol{A}_{3,1-4} & \boldsymbol{A}_{3,5}\end{array}\right]$, and $\boldsymbol{A}_{3,1-4}$ can be further referred to as $\left[\begin{array}{cccc}\boldsymbol{A}_{3,1} & \boldsymbol{A}_{3,2} & \boldsymbol{A}_{3,3} & \boldsymbol{A}_{3,4}\end{array}\right]$. Note that $\boldsymbol{A}_{3,1}$, $\boldsymbol{A}_{3,2}$, $\boldsymbol{A}_{3,3}$, $\boldsymbol{A}_{3,4}$, and $\boldsymbol{A}_{3,5}$ here represent the block matrices of $\boldsymbol{A}_3$, corresponding to $\boldsymbol{s}_1$, $\boldsymbol{x}_1$, $\boldsymbol{s}_2$, $\boldsymbol{s}_3$, and $\boldsymbol{x}_3$, respectively. In (30) and (31), $\boldsymbol{s}_2$, $\boldsymbol{x}_3^j$, and $\boldsymbol{\lambda}^j$ are the variables. Thus, the number of bilinear terms in (30) will be determined by the amount of nonzero terms in $\boldsymbol{A}_{3,3}$ and $\boldsymbol{A}_{3,5}$, while the number of bilinear terms in (31) will be determined by the amount of nonzero terms in $\boldsymbol{A}_{3,3}$ only.

$\boldsymbol{A}_{3,3}$ is a relatively sparse matrix, and according to (13)–(19), (22)–(23), and (25)–(27), the number of nonzero terms in $\boldsymbol{A}_{3,3}$

and $\boldsymbol{A}_{3,5}$ can be derived as follows:

$$\mathrm{N}_{\boldsymbol{A}_{3,3}} = 4\mathrm{card}(\mathcal{L}) \tag{32}$$

$$\mathrm{N}_{\boldsymbol{A}_{3,5}} = 12\mathrm{card}(\mathcal{L}) + 5\mathrm{card}(\mathcal{G}) + 6\mathrm{card}(\mathcal{B}), \tag{33}$$

where $\mathrm{card}(\mathcal{L})$, $\mathrm{card}(\mathcal{G})$, and $\mathrm{card}(\mathcal{B})$ represent the number of transmission lines, generators, and buses, respectively.

The number of bilinear terms in (30) is $\mathrm{N}_{\boldsymbol{A}_{3,3}} + \mathrm{N}_{\boldsymbol{A}_{3,5}}$, while the number in (31) is $\mathrm{N}_{\boldsymbol{A}_{3,3}}$, which means that much fewer bilinear terms will be introduced if the SDT is applied to the RoMIO model. Furthermore, the above difference is only for one calculation of (MP-II), and this calculation will be repeated several times for one calculation of (SP-I), while several calculations of (SP-I) will be required to solve the whole problem. Due to this cumulative effect, the difference in the number of bilinear terms will be greatly enlarged.

Thus, from an efficiency point of view, we propose using the SDT in our solution methodology because it could provide better computational efficiency for the RoMIO model, and this will be validated in Section V.

A linearization technique to deal with the bilinear terms induced by the SDT is provided as follows:

$$\begin{cases} y = \lambda s \\ \lambda \in \mathbb{R}_{\geq 0} \\ s \in \{0,1\} \end{cases} \Longleftrightarrow \begin{cases} y \geq 0 \\ y \leq \lambda \\ y \leq Ms \\ y \geq \lambda - M(1-s) \\ \lambda \in \mathbb{R}_{\geq 0} \\ s \in \{0,1\} \end{cases} \tag{34}$$

where y is a newly introduced variable, M is a large number, $\lambda \in \mathbb{R}_{\geq 0}$ and $s \in \{0,1\}$ represent the elements of decision variables $\boldsymbol{\lambda}^j$ and $\boldsymbol{s}_2$ respectively.

V. Illustrated Cases

We apply case studies on three different systems here, including a modified version of the PJM five-bus system, the IEEE one-area RTS-96 system, and the IEEE three-area RTS-96 system. The effectiveness of the proposed integrated resilience response will be verified, and the efficiency of the proposed SDT-based solution methodology will be investigated. We note that the emergency state decision making (i.e., the RoMIO-E model), as we previously stated in Section III-D, is a classical mixed-integer linear programming problem, and it can be directly and efficiently solved using the state-of-the-art MIP solvers. Thus we will focus on verifying the efficiency of the proposed solution methodology to solve the entire RoMIO model for the preventive state decision making. All the tests here are carried out on a 2.90-GHz Intel(R) Core(TM) i7-4600M based laptop, and Gurobi 6.5 [37] is used as the MIP solver with optimality tolerance set to be 1×10^{-3}. The maximum time limit for preventive state decision making is set as 1 hour, and "NA" indicates the methodology fails to solve the problem within the maximum time limit.

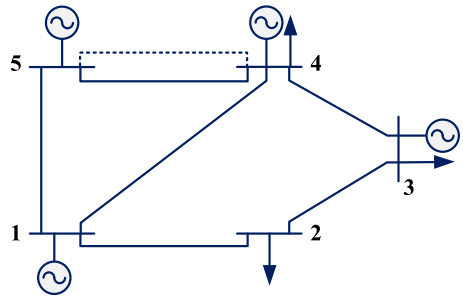

Fig. 3. The PJM five-bus system. Note that the dashed line in the figure represent the OSL in the preventive state.

TABLE I
Load Shed of the PJM Five-Bus System Under Different K^b

K^b	Load shed (MW)			
	PR	ER	IRR	IRR-TS
1	×	189	39	0
2	×	429	300	300
3	×	639	489	300
4	×	639	489	489
5	×	688	638	489
6	×	688	638	638
7	×	688	638	638

A. PJM Five-Bus System

The PJM five-bus system [38], depicted in Fig. 3, has four generators, three loads, and seven transmission lines (including one OSL in the preventive state). The system data we use are given in Appendix A. The ramp-up capacity in the emergency state is set to be 25% of that in the preventive state. The quantity limits for both ISLs switch off and OSLs switch on in preventive and emergency states are set to be the number of OSLs in the preventive state.

As previously stated, independent preventive respovvnse (referred to as "PR") includes generator re-dispatch in the preventive state, and independent emergency response (referred to as "ER") includes generator re-dispatch and load shedding in the emergency state; we will use them as benchmarks for our case studies. Based on the PR and ER, we will investigate the benefits of the integrated resilience response (referred to as "IRR"), which includes generator re-dispatch in the preventive state, and generator re-dispatch and load shedding in the emergency state. Furthermore, we will also investigate the benefits of the IRR with topology switching in both preventive and emergency states (referred to as "IRR-TS").

Table I gives the load shed with the PR, ER, IRR, and IRR-TS when the estimated maximum number of damaged transmission lines (i.e., K^b) varies. Here, "×" indicates that the response strategy cannot keep the generation-demand balance after disasters unfold.

From Table I, it can be seen that the PR fails to keep the power balance in all of the seven cases. This is because independent preventive response aims to withstand contingencies with only pre-disturbance strategies, and this will not work under severe

TABLE II
TOTAL COST AND OPERATING COST OF THE PJM FIVE-BUS SYSTEM UNDER DIFFERENT K^b

K^b	Total cost ($)			Operating cost ($)		
	ER	IRR	IRR-TS	ER	IRR	IRR-TS
1	206 520	59 945	16 463	17 520	20 945	16 463
2	446 520	320 315	316 163	17 520	20 315	16 163
3	656 520	509 077	320 315	17 520	20 077	20 315
4	656 520	509 637	508 970	17 520	20 637	19 970
5	705 520	655 675	509 637	17 520	17 675	20 637
6	705 520	655 675	655 375	17 520	17 675	17 375
7	705 520	655 675	655 375	17 520	17 675	17 375

TABLE III
LOAD SHED OF THE PJM FIVE-BUS SYSTEM UNDER DIFFERENT $P_g^{c,\max}$

$P_g^{c,\max}$	Load shed (MW)		
	ER	IRR	IRR-TS
20%	669	519	309
40%	662	512	302
60%	654	504	300
80%	647	497	300
100%	639	489	300
120%	632	482	300
140%	624	474	300
160%	617	467	300
180%	609	459	300

disturbances like natural disasters. This confirms the necessity of emergency response to keep the power balance against natural disasters.

It can also been observed that while the ER could keep the power balance against natural disasters, much more load will have to be shed, compared to the IRR or IRR-TS. For example, when $K^b = 1$, the ER has to shed 189 MW to keep the power balance, but the IRR has to shed only 39 MW, and the IRR-TS does not have to shed any load. This shows that integrated resilience response is preferable to both independent preventive response and independent emergency response in terms of enhancing power grid resilience, and the power grid resilience could be further enhanced by utilizing topology switching in the integrated resilience response.

The total cost of the ER, IRR, and IRR-TS under different K^b and the corresponding operating cost in the preventive state are given in Table II. We can see that the total cost could be greatly reduced if we utilize the IRR or IRR-TS rather than the ER. For example, the total cost of the ER is \$206,520 when $K^b = 1$, but the total cost of the IRR is \$59,945 while the total cost of the IRR-TS is \$16,463. On the other hand, the operating cost of the IRR or IRR-TS does not increase a lot compared to the ER. In fact, we can see that the operating cost could even decrease if the IRR-TS is applied. For example, when $K^b = 2$, the operating cost is reduced from \$17,520 to \$16,163 by utilizing the IRR-TS rather than the ER. This confirms the cost-effectiveness of the integrated resilience response. We note that while the IRR and IRR-TS in some cases have the same load shed (please see Table I), the IRR-TS could have lower operating cost because the topology switching provides more flexibility to the system and the system could therefore be operated with lower cost. The operating cost of the ER keeps the same because the generator redispatch in the emergency state will not influence the operating cost in the preventive state.

We also investigate the influence of generator ramp-up capacity on power grid resilience here. The emergency state ramp-up capacity (i.e., $P_g^{c,\max}$) is investigated because it will depend on the disaster severity. The base values of the capacities are kept the same as that in Appendix A, and Table III gives the simulation results of the system with the ER, IRR, and IRR-TS when the emergency state ramp-up capacity varies from 20% to 180%. Here, K^b is assumed to be 3.

TABLE IV
COMPUTATIONAL TIME FOR IRR AND IRR-TS OF THE PJM FIVE-BUS SYSTEM UNDER DIFFERENT K^b

K^b	Solving IRR (s)		Solving IRR-TS (s)	
	KKT	SDT	KKT	SDT
1	0.576	0.514	2.470	1.119
2	1.281	1.016	1.837	1.405
3	0.691	0.516	1.936	1.340
4	1.172	1.034	0.936	0.721
5	0.892	0.827	1.588	1.362
6	0.451	0.421	0.957	0.546
7	0.452	0.420	0.482	0.407

From Table III, it can be seen that larger ramp-up capacities can cause less load to be shed in order to keep the power balance. Note that when the IRR-TS is applied, load shed is no longer reduced when the $P_g^{c,\max}$ is larger than 60% of the base value. This is because the load at Bus-2 is 300 MW, and when $K^b = 3$, this load cannot be served as long as Line 1-2 and Line 2-3 are damaged. In other words, the IRR-TS is not able to alleviate this situation with larger $P_g^{c,\max}$ here because the load shed is not caused by the output limit of generators.

Table IV gives the computational time to solve the IRR problem and IRR-TS problem with the KKT-based solution methodology and the SDT-based solution methodology. We can see that the proposed SDT-based methodology is always faster to solve either problem. But a big difference cannot be observed here because the PJM five-bus system is small. To further compare these two methodologies, we will conduct research on larger systems in the next subsections.

B. IEEE One-Area RTS-96 System

The IEEE one-area RTS-96 system is the first version of the IEEE Reliability Test System, which was developed to be a reference system to test and compare results from different power grid operation strategies. An updated version of the system can be found in [39], and we apply a slight modification to the transmission line data, which could be found in Appendix B. The modified system has 12 generators, 36 transmission lines

TABLE V
LOAD SHED OF THE IEEE ONE-AREA RTS-96 SYSTEM UNDER DIFFERENT K^b

K^b	Load shed (MW)			
	PR	ER	IRR	IRR-TS
1	×	739	64	0
2	×	1139	356	289
3	×	1242	590	356
4	×	1522	766	590
5	×	1772	1016	766
6	×	1772	1250	1016
7	×	1834	1303	1250
8	×	1834	1312	1303
9	×	1834	1366	1303
10	×	1850	1366	1312

TABLE VI
COMPUTATIONAL TIME FOR IRR AND IRR-TS OF THE IEEE ONE-AREA RTS-96 SYSTEM UNDER DIFFERENT K^b

K^b	Solving IRR (s)		Solving IRR-TS (s)	
	KKT	SDT	KKT	SDT
1	NA	1.12	NA	3.07
2	NA	1.78	NA	2.95
3	NA	4.30	NA	8.51
4	NA	9.34	NA	29.65
5	NA	8.82	NA	35.97
6	NA	8.18	NA	30.94
7	NA	19.87	NA	32.72
8	NA	19.12	NA	44.59
9	NA	22.88	NA	62.47
10	NA	40.56	NA	56.01

(including 34 ISLs and 2 OSLs in the preventive state), and 17 loads.

When K^b varies from 1 to 10, Table V gives the corresponding load shed of the system with the PR, ER, IRR, and IRR-TS.

From Table V, we can again see that independent preventive response is not able to keep the power balance even when $K^b = 1$. This emphasizes the necessity of applying emergency response against natural disasters. On the other hand, although independent emergency response could always keep the power balance with load shedding, a large portion of the load shed by the emergency response could be saved if we apply integrated resilience response, and the load shed could be further reduced if topology switching is utilized in the integrated resilience response. For example, when $K^b = 2$, the ER has to shed 1,139 MW to keep the power balance, but the IRR and IRR-TS have to shed only 356 MW and 289 MW respectively.

The total cost and operating cost of the ER, IRR, and IRR-TS here follow the same trend as that in Table II, thus they are not presented for simplicity. For the same reason, the load shed under different $P_g^{c,\max}$ is also not presented here.

The computational time to solve the IRR and IRR-TS under different K^b is provided in Table VI. From this table, it can be seen that the KKT-based solution methodology fails to solve any of the problems within the maximum time limit, but the proposed SDT-based methodology could efficiently solve all the cases for the IRR problem and IRR-TS problem. This confirms the efficiency of the proposed solution methodology. In addition, we can see that the computational time will approximately increase with the growth of K^b, and although the topology switching in the integrated resilience response further enhances the power grid resilience, it also increases the computational time. But, for the IEEE one-area RTS-96 system, both the IRR problem and IRR-TS problem can be efficiently solved by the proposed methodology, as the maximum time needed is 62.47 seconds.

TABLE VII
LOAD SHED OF THE IEEE THREE-AREA RTS-96 SYSTEM UNDER DIFFERENT K^b

K^b	Load shed (MW)			
	PR	ER	IRR	IRR-TS
1	×	1648	0	0
2	×	1941	289	289
3	×	2006	308	289
4	×	2275	603	NA
5	×	2376	866	NA
6	×	2437	1042	NA
7	×	2470	1303	NA
8	×	2499	1303	1303
9	×	2532	1366	1303
10	×	2532	1366	1303

C. IEEE Three-Area RTS-96 System

The IEEE three-area RTS-96 system is the latest version and largest one of the IEEE Reliability Test System. To investigate the computational efficiency of the proposed solution methodology on larger systems, here we perform a third case study on the IEEE three-area RTS-96 system. Each area of the system shares the same parameters as that in Section V-B, where we assume there are two OSLs in the preventive state in Area-A. The data for the interconnections between areas could be found in [40]. The modified system has in total 36 generators, 110 transmission lines, and 51 loads.

Table VII gives the load shed of the system with the PR, ER, IRR, and IRR-TS when K^b varies from 1 to 10. Note that "NA" in the table indicates that we fail to get the optimal solution within the maximum time limit.

The observations we made in previous case studies could also be seen in this system:

1) The independent preventive response cannot keep the power balance in any of the ten cases.
2) The independent emergency response could keep the power balance with load shedding.
3) Compared with the independent preventive response and independent emergency response, the integrated resilience response could greatly enhance the power grid resilience. And with topology switching in the integrated resilience response, the load shed could be further reduced. For example, when $K^b = 3$, we need to shed 2006 MW load to keep the power balance with the ER, but we only need to shed 308 MW if the IRR is applied and 289 MW if the IRR-TS is applied.

TABLE VIII
COMPUTATIONAL TIME FOR IRR AND IRR-TS OF THE IEEE THREE-AREA RTS-96 SYSTEM UNDER DIFFERENT K^b

K^b	Solving IRR (s)		Solving IRR-TS (s)	
	KKT	SDT	KKT	SDT
1	NA	3.87	NA	32.01
2	NA	5.70	NA	44.30
3	NA	20.51	NA	2657.27
4	NA	22.93	NA	NA
5	NA	27.44	NA	NA
6	NA	25.32	NA	NA
7	NA	17.14	NA	NA
8	NA	33.10	NA	131.66
9	NA	41.53	NA	466.17
10	NA	55.77	NA	1849.56

But we note that the resilience benefit of topology switching is smaller than that in the IEEE one-area RTS-96 system, because we have the same number of OSLs in the preventive state but the system is bigger now. This indicates that the benefits of topology switching could be limited when applying to large systems, as the number of OSLs in the preventive state will not increase with the growth of system scale in reality due to considerations such as financial constraints.

We also note that while we could get all the optimal solutions for the IRR problem, we fail to derive optimal solutions for the IRR-TS problem in four of the ten cases. This indicates that topology switching introduces too much computational burden to the RoMIO model. To better analyze this problem, we provide the computational time to solve the IRR and IRR-TS in Table VIII.

From Table VIII, the computational efficiency of the proposed SDT-based methodology over the KKT-based methodology could again be proved. In addition, it is seen that although the proposed solution methodology could quite efficiently solve the IRR problem (with no more than 1 minute), it needs much longer time to solve the IRR-TS problem. In fact, the proposed solution methodology cannot always derive the optimal solution for the IRR-TS problem within the maximum time limit. This indicates that with topology switching considered, the integrated resilience response problem will be much harder to solve.

VI. PRACTICAL IMPLICATIONS

Before implementing the integrated resilience response, a variety of practical implications should be taken into account.

The first issue is on the feasibility of the proposed resilience response in practice. While current practice in many areas indicates that preventive response and emergency response are not only possible but also being done, some may argue that employing emergency response, especially topology switching, after the damage of natural disasters is impractical because of potential threats to the power grid. This concern mainly lies on the dynamic process of power grids, as the focus of this paper is in fact on the system adequacy against natural disasters, and the analysis in this paper is from the steady state point of view. In other words, to reach a solid conclusion in practice, the presented

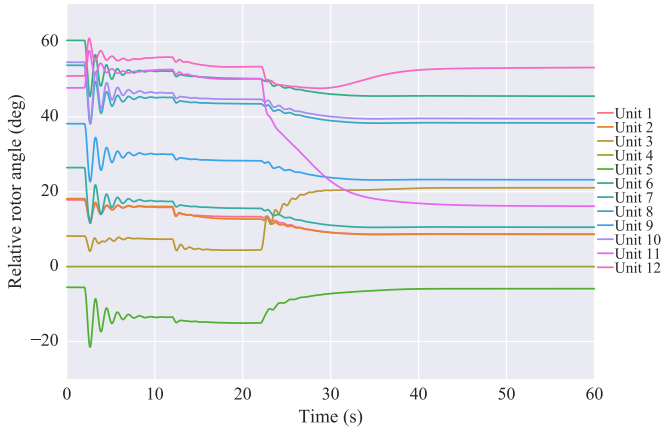

Fig. 4. Generator relative rotor angles of the representative case. Note that rotor angles here are relative to the slack generator (i.e., Unit 4 in [39]).

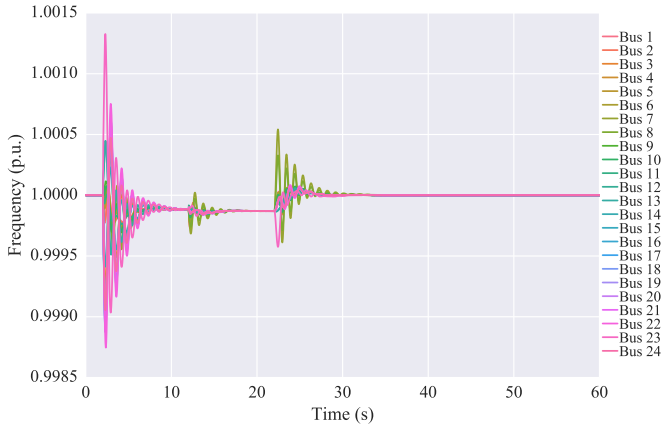

Fig. 5. Bus frequencies of the representative case.

model would need to be modified to include constraints ensuring dynamic feasibility, or the derived results need to be further validated via dynamic simulation.

Although detailed procedures for ensuring the dynamic feasibility is beyond the scope of this paper, we in this section provide the dynamic simulation using PSS/E as an example of checking whether the system can settle down after the employment of emergency response. The IEEE one-area RTS-96 system in this paper is chosen to be checked due to the availability of dynamic parameters. The data required to run the time-domain simulation could be found in [41], and the worst disaster scenario of the system with $K^b = 1$ is chosen as the representative case because other disaster scenarios require no topology switching in the emergency response. Following the convention in [42], we assume the damage occurs at $t = 2s$, then we perform topology switching 10 seconds later and generator re-dispatch after another 10 seconds (10 seconds is chosen in [42] to allow enough time for the breaker to operate and transients to damp down). Figs. 4 and 5 show the generator relative rotor angles and bus frequencies, respectively. It can be confirmed from Fig. 4 that the system could keep the transient stability during the dynamic process of emergency response, and Fig. 5 confirms that the

system frequency could be recovered in time. In summary, the emergency response is not necessarily antithetical to maintaining dynamic security.

In addition, although voltage problems can be associated with the process of rotor angles going out of step, voltage instability can occur where angle stability is not an issue [43]. Thus, the AC feasibility should also be studied and ensured before the results can be implemented.

Another issue is the solution time. This paper has proven that the integrated resilience response could greatly enhance the power grid resilience, but it should be noted that computational burden is therefore introduced. Though the problem of integrated resilience response without topology switching can be efficiently solved by the proposed solution methodology, when topology switching is included, how to solve the model efficiently in large systems is still an open question.

We also want to mention that several technologies are required to implement the integrated resilience response. For example, the transmission lines should be opened and closed quickly with sufficient situational awareness, and this requires further investment in communication and switching technology. Other technologies that could enhance the performances of generators or loads during either preventive state or emergency state [44]–[55] will also be beneficial to power grids, but we note that a full cost-benefit analysis should be conducted to support the decision making. With the development of these "smart grid" technologies, the power grids would be much smarter and stronger against natural disasters.

VII. Conclusion

This paper proposes an integrated resilience response (IRR) framework to enhance the power grid resilience against natural disasters. The core of the proposed IRR framework is a two-stage robust mixed-integer optimization (RoMIO) model, whose mathematical formulation and solution methodology are both provided. Through the research undertaken in this paper, we validate that the integrated resilience response is preferable to both independent preventive response and independent emergency response. In addition, we also prove that power grid resilience could be further enhanced by utilizing topology switching in the integrated resilience response.

The proposed IRR framework could incorporate other response strategies that are not investigated in this paper, as long as they can be modeled in the similar way to generator re-dispatch, load shedding, or topology switching. The IRR framework in this paper is proposed to enhance the power grid resilience against natural disasters, but they can also be easily modified to deal with other uncertainties that power grids face, for example, the cyber security and the massive integration of renewable energy resources.

Appendix A

The data of the PJM five-bus system are listed in Tables IX–XI. Among the transmission lines, Line 4-5B is the OSL in the preventive state.

TABLE IX
Generator Data of the PJM Five-Bus System

Bus	P_g^0 (MW)	$P_g^{\max}$ (MW)	$P_g^{a,\max}$ (MW)	c_g ($/MW)
1	210	210	60	15
3	323.49	520	100	30
4	0	200	50	40
5	466.51	600	150	10

TABLE X
Load Data of the PJM Five-Bus System

Bus	P_d (MW)	c_d ($/MW)
2	300	1000
3	300	1000
4	400	1000

TABLE XI
Transmission Line Data of the PJM Five-Bus System

Line	X_{ij} (p.u.)	$P_{ij}^{\max}$ (MW)	Line	X_{ij} (p.u.)	$P_{ij}^{\max}$ (MW)
1-2	0.0281	400	3-4	0.0297	300
1-4	0.0304	300	4-5A	0.0297	240
1-5	0.0064	300	4-5B	0.0297	240
2-3	0.0108	300			

Appendix B

The transmission line data of the IEEE one-area RTS-96 system are given in Table XII. Here, Line 14-16B and Line 15-21B are the OSLs in the preventive state.

TABLE XII
Transmission Line Data of the IEEE One-Area RTS-96 System

Line	X_{ij} (p.u.)	$P_{ij}^{\max}$ (MW)	Line	X_{ij} (p.u.)	$P_{ij}^{\max}$ (MW)
1-2	0.0146	175	11-14	0.0426	500
1-3	0.2253	175	12-13	0.0488	500
1-5	0.0907	350	12-23	0.0985	500
2-4	0.1356	175	13-23	0.0884	250
2-6	0.205	175	14-16A	0.0594	250
3-9	0.1271	175	14-16B	0.0594	500
3-24	0.084	400	15-16	0.0172	500
4-9	0.111	175	15-21A	0.0249	400
5-10	0.094	350	15-21B	0.0249	600
6-10	0.0642	175	15-24	0.0529	500
7-8	0.0652	350	16-17	0.0263	500
8-9	0.1762	175	16-19	0.0234	500
8-10	0.1762	175	17-18	0.0143	500
9-11	0.084	400	17-22	0.1069	500
9-12	0.084	400	18-21	0.0132	1000
10-11	0.084	400	19-20	0.0203	1000
10-12	0.084	400	20-23	0.0112	1000
11-13	0.0488	500	21-22	0.0692	500

References

[1] F. Estrada, W. Botzen, and R. Tol, "Economic losses from US hurricanes consistent with an influence from climate change," *Nature Geosci.*, vol. 8, pp. 880–884, Nov. 2015.

[2] A. Kenward and U. Raja, "Blackout: Extreme weather, climate change and power outages," Tech. Rep., Apr. 2014. [Online]. Available: http://www.ourenergypolicy.org/wp-content/uploads/2014/04/climate-central.pdf

[3] Executive Office of the President, "Economic Benefits of Increasing Electric Grid Resilience to Weather Outages," Tech. Rep., Aug. 2013. [Online]. Available: http://energy.gov/sites/prod/files/2013/08/f2/Grid%20Resiliency%20Report FINAL.pdf

[4] National Research Council, *The Resilience of the Electric Power Delivery System in Response to Terrorism and Natural Disasters: Summary of a Workshop*. Washington, DC, USA: The National Academies Press, 2013.

[5] M. Panteli and P. Mancarella, "Influence of extreme weather and climate change on the resilience of power systems: Impacts and possible mitigation strategies," *Electr. Power Syst. Res.*, vol. 127, pp. 259–270, Jun. 2015.

[6] M. Panteli and P. Mancarella, "The grid: stronger, bigger, smarter?: Presenting a conceptual framework of power system resilience," *IEEE Power Energy Mag.*, vol. 13, no. 3, pp. 58–66, Apr. 2015.

[7] Y. Wang, C. Chen, J. Wang, and R. Baldick, "Research on resilience of power systems under natural disasters—A review," *IEEE Trans. Power Syst.*, vol. 31, no. 2, pp. 1604–1613, Mar. 2016.

[8] L. Fisher, "Disaster responses: More than 70 ways to show resilience," *Nature*, vol. 518, no. 7537, pp. 35–35, Feb. 2015.

[9] T. Liacco, "The adaptive reliability control system," *IEEE Trans. Power App. Syst.*, vol. 5, no. PAS-86, pp. 517–531, May 1967.

[10] NERC, "FAC-003-3—Transmission Vegetation Management," May 2012. [Online]. Available: http://www.nerc.com/files/FAC-003-3.pdf

[11] W. Yuan, J. Wang, F. Qiu, C. Chen, C. Kang, and B. Zeng, "Robust optimization-based resilient distribution network planning against natural disasters," *IEEE Trans. Smart Grid*, vol. 7, no. 6, pp. 2817–2826, Nov. 2016.

[12] PJM State & Member Training Dept., "Elements of a System Restoration," Tech. Rep., Jul. 2012. [Online]. Available: https://www.pjm.com/~/media/training/nerc-certifications/sr-systemrestoration.ashx

[13] C. Chen, J. Wang, F. Qiu, and D. Zhao, "Resilient distribution system by microgrids formation after natural disasters," *IEEE Trans. Smart Grid*, vol. 7, no. 2, pp. 958–966, Mar. 2016.

[14] Y. Wen, W. Li, G. Huang, and X. Liu, "Frequency dynamics constrained unit commitment with battery energy storage," *IEEE Trans. Power Syst.*, vol. 31, no. 6, pp. 5115–5125, Nov. 2016.

[15] N. Fan, D. Izraelevitz, F. Pan, P. Pardalos, and J. Wang, "A mixed integer programming approach for optimal power grid intentional islanding," *Energy Syst.*, vol. 3, no. 1, pp. 77–93, Jan. 2012.

[16] M. Golari, N. Fan, and J. Wang, "Two-stage stochastic optimal islanding operations under severe multiple contingencies in power grids," *Electr. Power Syst. Res.*, vol. 114, pp. 68–77, Apr. 2014.

[17] M. Golari, N. Fan, and J. Wang, "Large-scale stochastic power grid islanding operations by line switching and controlled load shedding," *Energy Syst.*, pp. 1–21, Jul. 2016.

[18] P. Trodden, W. Bukhsh, A. Grothey, and K. McKinnon, "MILP formulation for controlled islanding of power networks," *Int. J. Elect. Power Energy Syst.*, vol. 45, no. 1, pp. 501–508, Feb. 2013.

[19] P. Trodden, W. Bukhsh, A. Grothey, and K. McKinnon, "Optimization-based islanding of power networks using piecewise linear ac power flow," *IEEE Trans. Power Syst.*, vol. 29, no. 3, pp. 1212–1220, May 2014.

[20] M. Panteli, D. Trakas, P. Mancarella, and N. Hatziargyriou, "Boosting the power grid resilience to extreme weather events using defensive islanding," *IEEE Trans. Smart Grid*, vol. 7, no. 6, pp. 2913–2922, Nov. 2016.

[21] E. Fisher, R. O'Neill, and M. Ferris, "Optimal transmission switching," *IEEE Trans. Power Syst.*, vol. 23, no. 3, pp. 1346–1355, Aug. 2008.

[22] K. Hedman, R. O'Neill, E. Fisher, and S. Oren, "Optimal transmission switching with contingency analysis," *IEEE Trans. Power Syst.*, vol. 24, no. 3, pp. 1577–1586, Aug. 2009.

[23] A. Delgadillo, J. Arroyo, and N. Alguacil, "Analysis of electric grid interdiction with line switching," *IEEE Trans. Power Syst.*, vol. 25, no. 2, pp. 633–641, May 2010.

[24] L. Zhao and B. Zeng, "Vulnerability analysis of power grids with line switching," *IEEE Trans. Power Syst.*, vol. 28, no. 3, pp. 2727–2736, Aug. 2013.

[25] F. Qiu and J. Wang, "Chance-constrained transmission switching with guaranteed wind power utilization," *IEEE Trans. Power Syst.*, vol. 30, no. 3, pp. 1270–1278, May 2015.

[26] M. Jabarnejad, J. Wang, and J. Valenzuela, "A decomposition approach for solving seasonal transmission switching," *IEEE Trans. Power Syst.*, vol. 30, no. 3, pp. 1203–1211, May 2015.

[27] A. Wagaman, "PPL Nearing Completion of Backup Transmission Line in Emmaus, Upper Milford," Jan. 2016. [Online]. Available: http://www.mcall.com/news/local/eastpenn/mc-emmaus-new-ppl-transmission-line-20160119-story.html

[28] NYISO Energy Market Operations, "Outage Scheduling Manual," Tech. Rep., Jul. 2015. [Online]. Available: http://www.nyiso.com/public/webdocs/markets_operations/documents/Manuals_and_Guides/Manuals/Operations/outage_sched_mnl.pdf

[29] PJM System Operations Division, "PJM Manual 13: Emergency Operations," Tech. Rep., Jan. 2016. [Online]. Available: http://www.pjm.com/~/media/documents/manuals/m13.ashx

[30] G. Tonn, S. Guikema, C. Ferreira, and S. Quiring, "Hurricane Isaac: A longitudinal analysis of storm characteristics and power outage risk," *Risk Anal.*, vol. 36, no. 10, pp. 1936–1947, Jan. 2016.

[31] M. Panteli, "Impact of ICT reliability and situation awareness on power system blackouts," Ph.D. dissertation, Univ. Manchester, Manchester, U.K., 2013.

[32] M. Panteli, P. Crossley, D. Kirschen, and D. Sobajic, "Assessing the impact of insufficient situation awareness on power system operation," *IEEE Trans. Power Syst.*, vol. 28, no. 3, pp. 2967–2977, Aug. 2013.

[33] M. Panteli and D. Kirschen, "Situation awareness in power systems: Theory, challenges and applications," *Electr. Power Syst. Res.*, vol. 122, pp. 140–151, Jan. 2015.

[34] P. Ruiz, "Reserve valuation in electric power systems," Ph.D. dissertation, Univ. Illinois Urbana-Champaign, Ann Arbor, MI, USA, 2008.

[35] J. Simonoff, C. Restrepo, and R. Zimmerman, "Risk-management and risk-analysis-based decision tools for attacks on electric power," *Risk Anal.*, vol. 27, no. 3, pp. 547–570, Jun. 2007.

[36] L. Zhao and B. Zeng, "An exact algorithm for two-stage robust optimization with mixed integer recourse problems, "Tech. Rep., Jan. 2012. [Online]. Available: http://http://www.optimization-online.org/DB_FILE/2012/01/3310.pdf

[37] Gurobi Optimization, Inc., "Gurobi optimizer reference manual," 2016. [Online]. Available: http://www.gurobi.com, 2016.

[38] F. Li and R. Bo, "Small test systems for power system economic studies," in *Proc. 2010 IEEE PES General Meeting*, Jul. 2010, pp. 1–4.

[39] C. Ordoudisa, P. Pinsona, J. Moralesb, and M. Zugnob, "An updated version of the IEEE RTS 24-bus system for electricity market and power system operation studies," Tech. Rep., 2016. [Online]. Available: http://orbit.dtu.dk/files/120568114/An_Updated_Version_of_the_IEEE_RTS_24Bus_System_for_Electricty_Market_an....pdf

[40] C. Grigg *et al.*, "The IEEE reliability test system-1996. A report prepared by the Reliability Test System Task Force of the Application of Probability Methods Subcommittee," *IEEE Trans. Power Syst.*, vol. 14, no. 3, pp. 1010–1020, Aug. 1999.

[41] J. Conto, "Dynamics networks 4 PSSE," 2016. [Online]. Available: https://drive.google.com/open?id=0B7uS9L2Woq_7YzYzcGhXT2VQYXc&authuser=0

[42] G. Huang, W. Wang, and J. An, "Stability issues of smart grid transmission line switching," in *Proc. 19th IFAC World Congr.*, Aug. 2014, pp. 7305–7310.

[43] K. Prabha, *Power System Stability and Control*. New York, NY, USA: McGraw-Hill, 1994.

[44] H. Ye and Z. Li, "Robust security-constrained unit commitment and dispatch with recourse cost requirement," *IEEE Trans. Power Syst.*, vol. 31, no. 5, pp. 3527–3536, Sep. 2016.

[45] G. Karady and J. Gu, "A hybrid method for generator tripping," *IEEE Trans. Power Syst.*, vol. 17, no. 4, pp. 1102–1107, Nov. 2002.

[46] Z. Wang, X. Song, H. Xin, D. Gan, and K. Wong, "Risk-based coordination of generation rescheduling and load shedding for transient stability enhancement," *IEEE Trans. Power Syst.*, vol. 28, no. 4, pp. 4674–4682, Nov. 2013.

[47] S. Padron, M. Hernandez, and A. Falcón, "Reducing under-frequency load shedding in isolated power systems using neural networks. Gran Canaria: A case study," *IEEE Trans. Power Syst.*, vol. 31, no. 1, pp. 63–71, Jan. 2016.

[48] Z. Wang and J. Wang, "Self-healing resilient distribution systems based on sectionalization into microgrids," *IEEE Trans. Power Syst.*, vol. 30, no. 6, pp. 3139–3149, Nov. 2015.

[49] M. Mansour, L. Alberto, and R. Ramos, "Preventive control design for voltage stability considering multiple critical contingencies," *IEEE Trans. Power Syst.*, vol. 31, no. 2, pp. 1517–1525, Mar. 2016.

[50] B. Hoseinzadeh, F. Silva, and C. Bak, "Adaptive tuning of frequency thresholds using voltage drop data in decentralized load shedding," *IEEE Trans. Power Syst.*, vol. 30, no. 4, pp. 2055–2062, Jul. 2015.

[51] J. Qi, S. Mei, and F. Liu, "Blackout model considering slow process," *IEEE Trans. Power Syst.*, vol. 28, no. 3, pp. 3274–3282, Aug. 2013.
[52] J. Qi, I. Dobson, and S. Mei, "Towards estimating the statistics of simulated cascades of outages with branching processes," *IEEE Trans. Power Syst.*, vol. 28, no. 3, pp. 3410–3419, Aug. 2013.
[53] J. Qi, K. Sun, and S. Mei, "An interaction model for simulation and mitigation of cascading failures," *IEEE Trans. Power Syst.*, vol. 30, no. 2, pp. 804–819, Mar. 2015.
[54] J. Qi, W. Ju, and K. Sun, "Estimating the propagation of interdependent cascading outages with multi-type branching processes," *IEEE Trans. Power Syst.*, vol. 32, no. 2, pp. 1212–1223, Mar. 2017.
[55] G. Andersson *et al.*, "Causes of the 2003 major grid blackouts in north america and europe, and recommended means to improve system dynamic performance," *IEEE Trans. Power Syst.*, vol. 20, no. 4, pp. 1922–1928, Nov. 2005.

Gang Huang (S'15) is currently working toward the Ph.D. degree in electrical engineering at Zhejiang University, Hangzhou, Zhejiang, China. During 2015–2016, he was a visiting Ph.D. student with the Energy Systems Division, Argonne National Laboratory, Argonne, IL, USA.

His primary research interests are centered around system resilience and mathematical optimization currently with applications in energy systems and smart grid. He received a Chinese Government Scholarship in 2015.

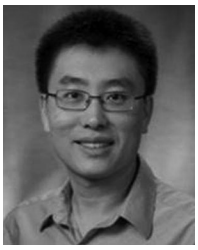

Jianhui Wang (M'07–SM'12) received the Ph.D. degree in electrical engineering from Illinois Institute of Technology, Chicago, IL, USA, in 2007.

Dr. Wang is currently an Associate Professor in the Department of Electrical Engineering, Southern Methodist University, Dallas, TX, USA. He also holds a joint appointment as the Section Lead for Advanced Power Grid Modeling in the Energy Systems Division, Argonne National Laboratory, Argonne, IL, USA.

Dr. Wang is the secretary of the IEEE Power & Energy Society (PES) Power System Operations, Planning & Economics Committee. He is an Associate Editor of the *Journal of Energy Engineering* and an editorial board member of *Applied Energy*. He has held visiting positions in Europe, Australia and Hong Kong including a VELUX Visiting Professorship at the Technical University of Denmark (DTU). He is the Editor-in-Chief of the IEEE TRANSACTIONS ON SMART GRID and an IEEE PES Distinguished Lecturer. He received the IEEE PES Power System Operation Committee Prize Paper Award in 2015.

Chen Chen (M'13) received the Ph.D. degree in electrical engineering from Lehigh University, Bethlehem, PA, USA, in 2013.

During 2013–2015, he worked as a Postdoctoral Researcher at the Energy Systems Division, Argonne National Laboratory, Argonne, IL, USA. He is currently a Computational Engineer in the Energy Systems Division, Argonne National Laboratory. His primary research interests include optimization, communications and signal processing for smart electric power systems, cyber-physical system modeling for smart grids, and power system resilience. He is an Editor of the IEEE TRANSACTIONS ON SMART GRID and the IEEE POWER ENGINEERING LETTERS.

Junjian Qi (S'12–M'13) received the Ph.D. degree in electrical engineering from Tsinghua University, Beijing, China, in 2013.

He is currently a Postdoctoral Appointee at the Energy Systems Division, Argonne National Laboratory, Argonne, IL, USA, and a joint appointed Argonne Staff at the Computation Institute, University of Chicago, Chicago, IL, USA. He was a Visiting Scholar at the Iowa State University, Ames, IA, USA, in February–August 2012, and a Research Associate in the Department of Electrical Engineering and Computer Science, University of Tennessee, Knoxville, TN, USA, during September 2013–January 2015. His research interests include cascading blackouts, power system dynamics, state estimation, synchrophasors, voltage control, and cybersecurity. Dr. Qi is the Secretary of the IEEE Task Force on "Voltage Control for Smart Grids."

Chuangxin Guo (M'10–SM'14) received the Ph.D. degree in electrical engineering from Huazhong University of Science and Technology, Wuhan, Hubei, China, in 1997.

He is currently a Professor and the Vice Dean with the College of Electrical Engineering, Zhejiang University, Hangzhou, Zhejiang, China. Prior to joining Zhejiang University, he worked as the Director of Beijing Dongfang Electronics Research Institute and the Deputy Chief Engineer of Dongfang Electronics Co., Ltd. During August–October 2012, he was a Senior Visiting Scholar at the University of Washington, Seattle, WA, USA.